Journal of Southeast University (English Edition) Vol. 28, No. 2, pp. 169 - 174 June 2012 ISSN 1003—7985

Date palm kernel-based GAC and its dynamic modeling of residual chlorine breakthrough curve in multimedia filter

Rusul Naseer Mohammed Lü Xiwu Saad Abualhail

(School of Energy and Environment, Southeast University, Nanjing 210096, China)

Abstract: First, the date palm kernel is used to produce granular activated carbon (GAC) by a physiochemical activation process. The process involves six steps: washing, drying, crushing, sieving, carbonization, and activation. Secondly, the ability of the produced GAC to remove pollutants is examined through batch experiments of residual chlorine adsorption whereas the equilibrium isotherm experimental data are tested for the Langmuir and Freundlich isotherms equations. Thirdly, the experimental and theoretical study of dynamic adsorption process and the effect of major operating parameters on dynamic adsorption are investigated. The results show that the Langmuir isotherm gives the best fitting to experimental data, which indicates that the residual chlorine adsorption can be characterized by mono layer adsorption behavior. The produced GAC has a great potential as an adsorbent for residual chlorine in water systems and it can compete favorably with the conventional adsorbents. The Thomas extended model with combined mass transfer resistances is used for verifying the experimental results and the results show that the proposed model coincides well with the experimental data of the dynamic adsorption process.

Key words: residual chlorine adsorption; granuler activated carbon (GAC); model isotherm; multimedia filter; date palm kernel

doi: 10.3969/j.issn.1003 - 7985.2012.02.007

Activated carbon is extensively used to remove pollutants from gaseous and liquid process streams. It is well known that activated carbon is produced from a wide variety of carbon rich raw materials including wood, coal, peat, and coconut shells. In the water treatment industry, activated carbon has been used as a filtration medium to improve water quality since centuries, and large amounts of activated carbon are used annually for this purpose. The wood, coal, peat and coconut shells are relatively inexpensive and economical starting materials as sources for the production of activated carbon. Researchers have studied the production of activated carbon from palm-tree cobs[1], plum kernels[2], cassava peel[3], bagasse[4], jute fiber[5], rice husks[6], olive stones[7], fruit stones and nutshells[8]. The advantage of using agricultural by-products as raw materials for manufacturing activated carbon is that these raw materials are renewable and potentially less expensive to manufacture date palm kernel. Activated carbon is produced by chemical or physical activation of carbonaceous materials[9]. The features of carbons such as porosity, surface area, density, and mechanical stability govern the use of activated carbons as adsorbents[10]. The adsorption mechanism of activated carbon provides a highly efficient way to remove chlorine, although reaction rates may vary with chlorine concentration, type of residual, carbon particle size, pH, and organic matter[11]. Activated carbon is very effective in removing free chlorine from water[12] whereas the mechanism of removal employed by activated carbon for dechlorination is not the adsorption phenomena that occur for organic compound removal. Adsorption in a fixed bed column generally depends on the adsorption isotherm and the transport mechanisms in adsorbent particles as well as the operating conditions of the column, such as adsorbate inlet concentration, adsorbate flow rate, height of bed, and adsorbent particle diameter[13]. In this paper, a series of experiments are conducted with different operating conditions to examine the effect of GAC adsorbent on residual chlorine removal to predict the performance of adsorption processing in packed bed adsorption.

1 Material and Methods

1.1 Water characteristics

In the present study, the raw water used is taken from a water treatment plant. The physical and chemical properties of the raw water are examined as shown in Tab. 1.

1.2 Date palm kernel

The date palm kernel is used for the production of activated carbon throughout the experimental work. The basic compositions of the date palm kernel are given in Tab. 2[14]. It shows that the date palm kernel contains carbohydrates, so high-grade activated carbon is obtained from the date palm kernel due to its high carbon content, as shown in Tab. 3.

Received 2011-11-20.

Biographies: Rusul Naseer Mohammed (1985—), female, graduate; Lü Xiwu (corresponding author), male, doctor, professor, xiwulu@seu.edu.cn.

Foundation item: The National Natural Science Foundation of China (No. 51078074).

Citation: Rusul Naseer Mohammed, Lü Xiwu, Saad Abualhail. Date palm kernel-based GAC and its dynamic modeling of residual chlorine breakthrough curve in multimedia filter[J]. Journal of Southeast University (English Edition), 2012, 28(2): 169 - 174. [doi: 10.3969/j.issn.1003 - 7985.2012.02.007]

Tab. 1 Characteristics of raw water

Item	Value
$C_{Chlorides}/(mg \cdot L^{-1})$	123
$C_{HCO_3}/(mg \cdot L^{-1})$	165
Turbidity/NTU	10.1
$C_{TSS}/(mg \cdot L^{-1})$	11.2
EC $/(\mu S \cdot cm^{-1})$	909
$C_{SO_4}/(mg \cdot L^{-1})$	26
pH	7.4
$C_{Ca}/(mg \cdot L^{-1})$	88
$C_{Mg}/(mg \cdot L^{-1})$	34
$C_{Na}/(mg \cdot L^{-1})$	74
$C_{DO}/(mg \cdot L^{-1})$	7.1
$C_{Total\ hardness}/(mg \cdot L^{-1})$	288

Tab. 2 Basic compositions of date palm kernel[14]

Component	Percent/%
Moisture	5 to 10
Protein	5 to 7
Oil	7 to 10
Crude fibber	10 to 20
Carbohydrates	55 to 65
Ash	1 to 2

Tab. 3 Major components of date palm kernel %

Compounds	w_{Burned}	w_{Raw}
K_2CS_2	1.8	0.7
Amorphous phase	86.2	92
$KOH \cdot H_2O$	3	2.3
$H_4P_2O_7$		
$KBaP_3O_9 \cdot H_2O$	9	5

2 Experimental Setup

Production of GAC is one of the most important parts of this study. Different experimental conditions are investigated to achieve an activated carbon with optimum physical characteristics. This part of the study involves six steps: washing, drying, crushing, sieving, carbonization, and activation. In the first step, the kernels are initially washed with water to remove any impurities that may be found. In the second step, which is drying, the washed kernels are placed in an electrical oven for 3 h at 150 ℃ to remove the moisture content from the kernel. The third step is crushing. The kernels are crushed in a jaw crusher. In the fourth step, the crushed kernels are sieved in a sieve shaker for 20 min. In the carbonization step, the kernel is horizontally placed in the electrical furnace and subjected to an average temperature of 700 ℃ for 1.5 h at a heating rate of 20 ℃/min. For each experiment, 50 g of raw material is used. Samples are placed in the furnace, and then N_2 flow starts to purge the air in the tubular furnace for 10 min. After purging, the furnace is heated up till the chosen carbonization temperature is achieved, and this temperature is kept constant by the temperature controller of the furnace. The heating period is selected based on previous trials of different heating durations. It is observed that the brown color of the kernel persistently appears after the carbonization process when the heating duration is less than 1.5 h. In the last step, the process of activation, the nitrogen gas cylinder is replaced with a carbon dioxide cylinder, and heating is continued for another 1.5 h. The flow of carbon dioxide gas coming from the end of the tubular furnace passes through the kernel, forcing the formation of macropores. When the heating duration is raised to more than 1.5 h, it is observed that the kernel has begun to carbonize into ash. The dynamic adsorption process is carried out by a deep bed filter column with a height of 120 cm and a diameter of 80 cm. Several experiments are implemented by the changing of the characteristics of the GAC, the operation conditions and the feed concentration. The parameters are shown in Tab. 4.

Tab. 4 Experimental setup for residual chlorine adsorption

Parameter	Range
Initial chlorine concentration/$(mg \cdot L^{-1})$	2 to 3
Feed flow rate/$(cm^3 \cdot min^{-1})$	500 to 1 300
Height of bed/cm	5 to 30
Grain diameter of GAC/mm	1.5 to 2.36
Porosity of GAC	0.51 to 0.44

3 Mathematical Model

3.1 Equilibrium isotherm models

The first model used in this paper is the Langmuir model to simulate the batch experiment, which is recurrently expressed in terms of the weight of adsorbate on the surface[14], and it is given by

$$\frac{1}{q_A} = \frac{1}{Q} + \frac{1}{K'Q}\frac{1}{C_A} \tag{1}$$

where q_A is the equilibrium adsorption capacity; Q is the weight of adsorbate for complete monolayer; K' is the rate constant adsorption; C_A is the concentration of solute A.

The second model used in this paper is the Freundlich model where the general form of the adsorption is

$$q_A = K_f C_A^{1/n} \tag{2}$$

where K_f is the fluid-phase mass transfer coefficient; n is the Freundlich adsorption constant.

3.2 Breakthrough curves using Thomas model

3.2.1 Control of external film resistance (EFR)

Derivation of the adsorption described by the Langmuir model can be carried out in the following manner, and the rate of uptake is equal to the rate of adsorption minus the rate of adsorption[15]. Thus, for the adsorption of solute A,

$$\frac{\partial C_s}{\partial t} = K_a C(Q' - C_s) - K_d C_s \tag{3}$$

where $K' = K_a/K_d$; $Q' = ((1 + K'C_o)/(K'C_o))C_s^{\infty}$; K_a is the constant rate of adsorption; K_d is the constant rate of desorption; K' is the equilibrium constant; C_s^{∞} is the saturated concentration of solute A on the surface; C_s is the saturated concentration of the adsorbate.

Substituting Q' into Eq. (3), we obtain

$$\frac{\partial(C_s/C_s^\infty)}{\partial t}=\Delta_a\left[\frac{C}{C_o}\left(1-\frac{C_s}{C_s^\infty}\right)-\frac{1}{1+K'C_o}\frac{C_s}{C_s^\infty}\left(1-\frac{C}{C_o}\right)\right] \tag{4}$$

According to the Langmuir kinetics concept, Eq. (4) can be rewritten as

$$\frac{\partial(C_s/C_s^\infty)}{\partial t}=\Delta_a\left[\frac{C}{C_o}\left(1-\frac{C_s}{C_s^\infty}\right)-r^*\frac{C_s}{C_s^\infty}\left(1-\frac{C}{C_o}\right)\right] \tag{5}$$

where $\Delta_a=aK(1+K'C_o)/K'$, and $r^*=1/(1+K'C_o)$.

At EFR controlling,

$$\frac{\partial C_s}{\partial t}=\frac{aK_f(C-C_i)}{1-\varepsilon} \tag{6}$$

where a is the condensation coefficient; C_i is the initial concentration of adsorbate.

When the rate of adsorption equals zero, $C=C_i$ and $\partial(C_s/C_s^\infty)/\partial t=0$. Also, substituting Eq. (6) into Eq. (5), we can obtain

$$C_i=\frac{C_s}{C_s^\infty}r^*\frac{C_o}{1+C_s/C_s^\infty(r^*-1)} \tag{7}$$

According to the definition of C_i, Eq. (4) can be rewritten as

$$\frac{\partial(C_s/C_s^\infty)}{\partial t}=\frac{aK_fC_o}{C_s^\infty(1-\varepsilon)[1+C_s/C_s^\infty(r^*-1)]}\cdot\left[\frac{C}{C_o}\left(1-\frac{C_s}{C_s^\infty}\right)-r^*\frac{C_s}{C_s^\infty}\left(1-\frac{C}{C_o}\right)\right] \tag{8}$$

where ε is the void fraction.

3.2.2 Control of internal particle resistance (IPR)

The rate of adsorbate uptake is expressed as

$$\frac{\partial C_{As}}{\partial t}=aK_s(C_{Asi}-C_{As}) \tag{9}$$

where K_s is the solid-phase transfer coefficient; C_{Asi} is the interfacial concentration of solute A in solid phase.

$$\frac{\partial C_s}{\partial t}=aK_s(C_{si}-C_s) \tag{10}$$

$$C_{si}=\frac{C_s^\infty}{r^*-1}+r^*\frac{C_o}{C} \tag{11}$$

The differential equation in this case can be obtained by substituting C_{si} instead of C_s in Eq. (5) and substituting the relationship into Eq. (9). Therefore,

$$\frac{\partial(C_s/C_s^\infty)}{\partial t}=\frac{aK_sC_o}{r^*+C/C_o(r^*-1)}\cdot\left[\frac{C}{C_o}\left(1-\frac{C_s}{C_s^\infty}\right)-r^*\frac{C_s}{C_s^\infty}\left(1-\frac{C}{C_o}\right)\right] \tag{12}$$

or

$$\frac{\partial(C_s/C_s^\infty)}{\partial t}=\Delta_s\left[\frac{C}{C_o}\left(1-\left(\frac{C_s}{C_s^\infty}-r^*\frac{C_s}{C_s^\infty}\right)\left(1-\frac{C}{C_o}\right)\right)\right] \tag{13}$$

where Δ_s is the constant parameter, s^{-1}.

3.2.3 Combined internal and external resistances

For the case in which both the external film resistance and intraparticle resistance are important, the previous rate equations can be combined together[13]. Since the total rate of adsorbate uptake is equal to the total sum of all the rate equations, it can be shown that

$$\frac{\partial(C_s/C_s^\infty)}{\partial t}=\left[\frac{aK_fC_o}{C_s^\infty(1-\varepsilon)[1+(C_s/C_s^\infty)(r^*-1)]}+\frac{aK_s}{r^*+(C/C_o)(r^*-1)}\right]\left[\frac{C}{C_o}\left(1-\frac{C_s}{C_s^\infty}\right)-r^*\frac{C_s}{C_s^\infty}\left(1-\frac{C}{C_o}\right)\right] \tag{14}$$

$$\Delta=\frac{aK_fC_o}{C_s^\infty(1-\varepsilon)\left[1+\frac{C_s}{C_s^\infty}(r^*-1)\right]}+\frac{aK_s}{\left[r^*+\frac{C}{C_o}(r^*-1)\right]}$$

The dimensionless form of Eq. (14) can be expressed by defining bed-length and time parameters[16]. The dimensionless groups are

$$\beta_l=\frac{Z(1-\varepsilon)C_s^\infty\Delta}{\varepsilon U_zC_o} \tag{15}$$

$$\vartheta=\Delta\vartheta=\Delta\left(\vartheta-\frac{Z}{U_z}\right) \tag{16}$$

$$\bar{Q}=\frac{C_s}{C_s^\infty},\qquad \bar{X}=\frac{C}{C_o}$$

where β_l is the bed-length parameter; ϑ is the time parameter; Z is the bed height; U_z is the interstitial velocity; $\bar{X}$ and $\bar{Q}$ are the concentration parameters.

Substituting the dimensionless parameters into Eq. (14), we can obtain that

$$\frac{\partial\bar{Q}}{\partial\vartheta}=\bar{X}(1-\bar{Q})-r^*\bar{Q}(1-\bar{X}) \tag{17}$$

The axial diffusion is

$$\left(\frac{\partial\bar{Q}}{\partial\vartheta}\right)_\alpha=-\left(\frac{\partial\bar{X}}{\partial\alpha}\right)_\vartheta \tag{18}$$

Combining Eq. (17) with Eq. (18), we have

$$\frac{\partial\bar{Q}}{\partial\vartheta}=\bar{X}(1-\bar{Q})-r^*\bar{Q}(1-\bar{X}) \tag{19}$$

$$\frac{\partial\bar{X}}{\partial\alpha}=-\bar{X}(1-\bar{Q})-r^*\bar{Q}(1-\bar{X}) \tag{20}$$

The influent concentration at the entrance and the initial solute concentration in the bed are equal to zero at the fol-

lowing boundary conditions:

$$C_A = C_{Ao} \text{ at } Z = 0,\ X = 1,\ \text{and } \alpha = 0 \text{ for all } \vartheta$$

$$q_A = 0 \text{ at } t = Z/Uz,\ \bar{Q} = 0,\ \text{and } \vartheta = 0 \text{ for all } \alpha$$

The set of Eqs. (19) and (20) are solved using the Laplace transform method according to Ref. [17] for the concentrations of the fluid and solid phases,

$$\frac{C}{C_o} = \frac{\bar{\gamma}(r^*,\alpha,\vartheta)}{\bar{\gamma}(r^*,\alpha,\vartheta) + [1 - \gamma(r^*\alpha,\vartheta)\exp[(r^* - 1)(\vartheta - \alpha)]}$$

$$\frac{C_s}{C_s^\infty} = \frac{1 - \gamma\ (r^*,\vartheta,\alpha)}{\bar{\gamma}(r^*,\alpha,\vartheta) + [1 - \bar{\gamma}(r^*,\alpha,\vartheta)\exp[r^* - 1)(\vartheta - \alpha)]}$$

$$\bar{X}(m) = \frac{1 - \bar{\gamma}(r^*,\alpha,\vartheta)}{\gamma(r^*,\alpha,\vartheta) + [1 - \gamma(r^*,\alpha,\vartheta)\exp[r^* - 1)(\vartheta - \alpha)]} \quad (21)$$

where $\bar{\gamma}(\vartheta,\alpha) = 1 - \int_0^\alpha e^{-(\vartheta+\alpha)}\gamma_o(i\sqrt{4\alpha\vartheta})\,d\alpha$.

In this paper, a computer program is written in Matlab 7.0 to simulate the adsorption process in the multimedia filter based on the combined internal and external resistances as shown in Fig. 1.

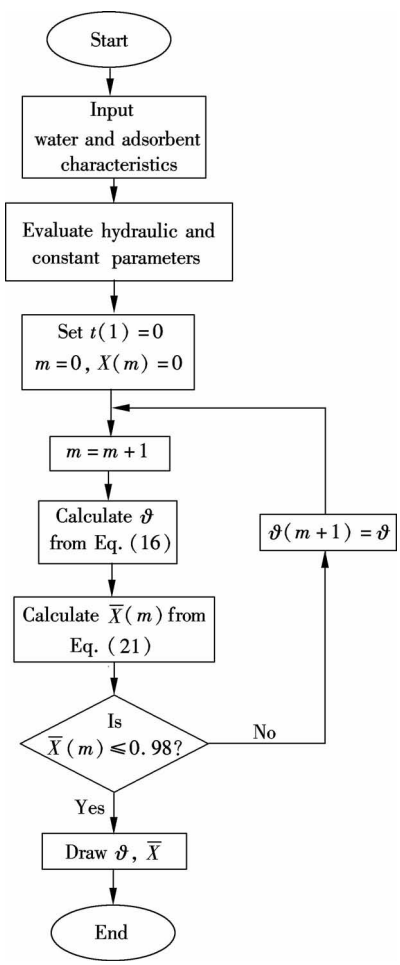

Fig. 1 Flow chart of the adsorption process

4 Results and Discussion

4.1 Equilibrium isothermal results

Batch experiments are performed to characterize the adsorption isotherms for both the produced GAC and the conventional GAC at 30 ℃. The results are analyzed using two different isotherm equations (see Fig. 2). The results show that the experimental data give a good fit with the Langmuir isotherm equation; thus, the description of the adsorption of residual chlorine on the GAC by the Langmuir isotherm equation is a pointer to the monolayer adsorption nature of the residual chlorine on GAC adsorbent. The equilibrium adsorption capacity q_A of the produced GAC obtained in the present study is compared with that of the conventional GAC for residual chlorine adsorption as shown in Fig. 3. The results show that the produced GAC has a great potential as an adsorbent for residual chlorine in water systems and can compete favorably with conventional adsorbents.

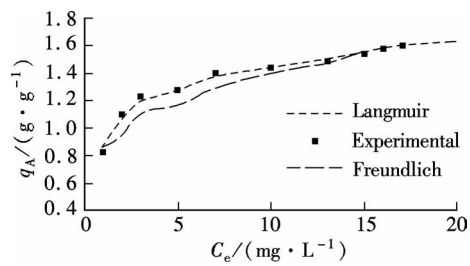

Fig. 2 Residual chlorine adsorption isotherm on conventional GAC

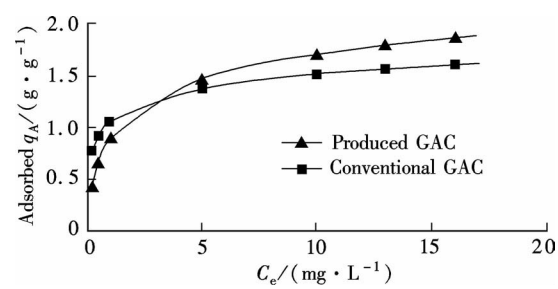

Fig. 3 Experimental adsorption equilibrium of residual chlorine on produced GAC and conventional GAC adsorbents

4.2 Adsorbent characterization

The adsorbent characteristics are measured and analyzed in this paper. The particle density of the produced GAC is 1.09 g/cm^3 which is greater than that of the particle density of the conventional GAC (0.411 g/cm^3), while the bulk density of the conventional GAC is 0.478 g/cm^3 which is greater than that of the bulk density of the produced GAC (0.433 g/cm^3). In addition, the produced GAC pores have larger porosity than the conventional GAC. Surface area test results indicate that it is possible to produce a compatible GAC from the date palm

kernel. The produced GAC has a larger surface area (700 m^2/g) in a few square meters, and a larger pore (0.631 cm^3/g) volume than the conventional GAC. Moreover, the surface area of the produced GAC may be increased by tuning the activation process variables. Also the results show that the surface of the produced GAC is more acidic. The surface acidity is due to the presence of carbon-oxygen surface chemical structures.

4.3 Simulation results

4.3.1 Effect of bed height

The effect of the bed height on the effluent adsorbate concentration is presented in Fig. 4. It is observed that as the bed height increases from 5 to 30 cm, the break point time increases from 50 to 250 min. This shows that at a smaller bed height, the effluent adsorbate concentration ratio increases more rapidly than that of a higher bed height. Furthermore, a smaller bed height corresponds to a lesser amount of adsorbent.

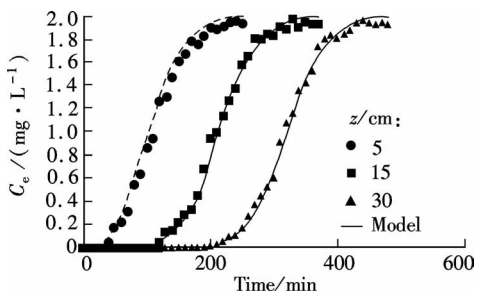

Fig. 4 Effect of GAC characteristics on adsorption breakthrough

4.3.2 Effect of inlet adsorbate concentration

Fig. 5 shows the effect of inlet residual chlorine concentration on the adsorption breakthrough. It is observed that as the inlet adsorbate concentration increases from 2 to 3 mg/L, the break point time decreases from 160 to 144 min. For a higher feed concentration, a steeper breakthrough curve is found because the lower mass transfer flux from the bulk solution to the adsorbent surface due to the weaker driving force.

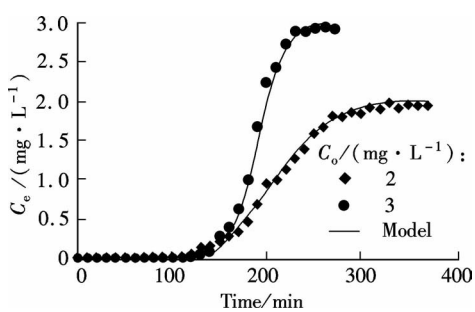

Fig. 5 Effect of inlet residual chlorine

4.3.3 Effect of flow rate on adsorption process

Fig. 6 shows that the break time appears earlier at a higher flow rate. On the other hand, the breakthrough curves are steeper at a higher flow rate. This is because the residence time of the solute in the column is not enough to reach adsorption equilibrium at a high flow rate, so the adsorbate solution leaves the column before equilibrium occurs. Furthermore, a fixed adsorption capacity of a bed based on the same driving force gives rise to a shorter time for saturation at a higher flow rate.

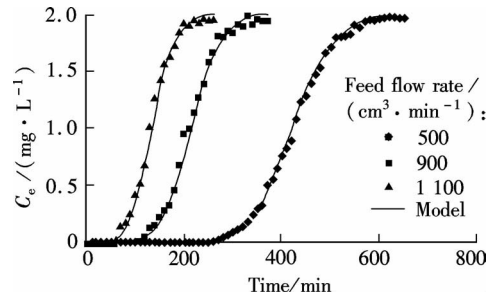

Fig. 6 Effect of flow rate on adsorption breakthrough for different grain sizes

4.3.4 Effect of particle diameter

Fig. 7 is a plot of predicted concentration-time profiles for different grain sizes while the other parameters are kept constant (the bed height of 15 cm, the inlet concentration of 2 mg/L and the flow rate of 700 cm^3/min). It reveals that as the particle diameter increases from 1.50 to 2.36 mm, the steepness of the breakthrough curve decreases. The break point time increases from 150 to 180 min. This can be explained as follows: As the diameter of the particle increases, the thickness of the stagnant film around the particles increases, and also the total length of the path inside the pores increases. Under these conditions, the overall kinetics of the process is slow, because it requires more time to reach the adsorption site where the diffusion path along the pores is long.

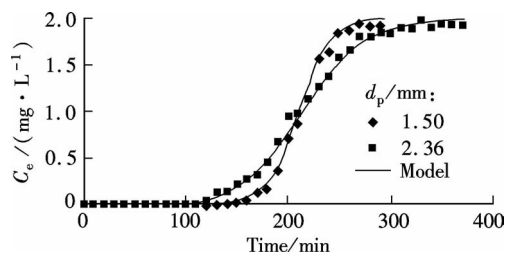

Fig. 7 Effect of particle diameter on adsorption breakthrough

5 Conclusion

In this paper, equilibrium isotherms as well as the dynamics of residual chlorine adsorption from raw water via produced GAC and conventional GAC adsorbents have been studied. The major observations based on these adsorptions experiments are stated below:

1) The date palm kernel is used for producing GAC via physiochemical activation process.

2) The produced GAC adsorbent pores has higher adsorption capacity than the conventional GAC.

3) The Langmuir isotherm model gives a better fitting with experimental data compared with the Freundlich isotherm model due to the characterization of the GAC by mono layer adsorption behavior.

4) The Thomas extended model with combined mass transfer resistances is used for analyzing and simulating

the adsorption of residual chlorine from tap water in a multimedia filter and the results show that the proposed model coincides well with the experimental data of the dynamic process.

5) A high removal efficiency of residual chlorine from chlorinated water can be obtained at a depth of 15 cm with a small grain size of 1.5 mm of the GAC. Furthermore, the model results can be used to design the GAC layer in the multimedia filter where the best operating parameters are predicated.

References

[1] Avom J, Mbadcam J K, Noubactep C, et al. Adsorption of methylene blue from an aqueous solution on to activated carbons from palm-tree cobs [J]. *Carbon*, 1997, **35**(3):365 - 369.

[2] Wu Feng-Chin, Tseng Ru-Ling, Juang Ruey-Shin. Pore structure and adsorption performance of the activated carbons from plum kernels [J]. *Journal of Hazardous Material*, 1999, **69**(3): 287 - 302.

[3] Rajeshwarisivaraj, Sivakumar S, Senthilkumar P, et al. Carbon from cassava peel, an agricultural waste, as an adsorbent in the removal of dyes and metal ions from aqueous solution [J]. *Bioresource Technology*, 2001, **80**(3): 233 - 235.

[4] Tsai W T, Chang C Y, Lin M C, et al. Adsorption of acid dye onto activated carbons prepared from agricultural waste bagasse by $ZnCl_2$ activation [J]. *Chemosphere*, 2001, **45**(1): 51 - 58.

[5] Senthilkumaar S, Varadarajan P R, Porkodi K, et al. Adsorption of methylene blue onto jute fiber carbon: kinetics and equilibrium studies [J]. *Colloid and Interface Science*, 2005, **284**(1): 78 - 82.

[6] Yalcin N, Sevinc V. Studies of the surface area and porosity of activated carbons prepared from rice husks[J]. *Carbon*, 2000, **38**(14): 1943 - 1945.

[7] El-Sheikh A H, Newman A P, Al-Daffaee H K, et al. Characterization of activated carbon prepared from a single cultivar of Jordanian olive stones by chemical and physiochemical techniques [J]. *Analytical and Applied Pyrolysis*, 2004, **71**(1):151 - 164.

[8] Aygün A, Yenisoy-Karakas S, Duman I. Production of granular activated carbon from fruit stones and nutshells and evaluation of their physical chemical and adsorption properties[J]. *Microporous and Mesoporous Materials*, 2003, **66**(2/3):189 - 195.

[9] Barreveld W H. Date palm products[M/OL]. [1993](2011-08-30). http://www.fao.org/docrep/t0681E/t0681E00.htm

[10] Salame I I, Bandosz J T. Comparison of the surface features of two wood-based activated carbons [J]. *Industrial and Engineering Chemistry Research*, 2000, **39**(2):301 - 306.

[11] Snoeyink V L, Suidan M T. Dechlorination by activated carbon and other reducing agents [C]// *Disinfection: Water and Wastewater*. Ann Arbor: Ann Arbor Science, 1975: 339 - 358.

[12] Potwora R. Chlorine and chloramine removal with activated carbon [J]. *Water Conditioning and Purification*, 2009(5):14 - 16.

[13] Hines A L, Maddox R N. *Mass transfer: fundamentals and applications* [M]. Upper Saddle River, NJ, USA: Prentice-Hall, 1985:460.

[14] Esmaeili A, Ghasemi S. Evaluation of the activated carbon prepared of algae marine Gracilaria for the biosorption of Ni (Ⅱ) from Aqueous Solutions [J]. *World Applied Sciences Journal*, 2009, **6**(4): 515 - 518.

[15] Tien C. *Adsorption calculations and modeling*[M]. Boston: Butterworth-Heinemann, 1994.

[16] Namasivayam C, Kavitha D. Removal of Congo Red from water by adsorption onto activated carbon prepared from coir pith an agricultural solid waste [J]. *Dyes and Pigments*, 2002, **54**(1): 47 - 58.

[17] Lightfoot E N, Sanchez-Palma R J. Edwards D O. *New chemical engineering separation techniques* [M]. New York: Wiley, 1962.

枣椰仁颗粒活性碳及其在多介质过滤器中余氯穿透曲线动态建模

Rusul Naseer Mohammed 吕锡武 Saad Abualhail

(东南大学能源与环境学院,南京 210096)

摘要:采用物化活化工艺,以枣椰仁为原材料制作颗粒活性碳(GAC),制作过程主要有6个步骤:清洗,烘干,粉碎,筛分,炭化和活化.通过小试对新型GAC去除余氯的特性进行了研究,并将实验结果与Langmuir和Freundlich等温方程进行了拟合.通过理论和实验分析,考察了主要运行参数对吸附动力的影响.结果表明:Langmuir等温方程与实验数据最为吻合,说明其对余氯吸附为单层吸附.新型GAC在余氯吸附方面具有巨大潜力,比传统的吸附剂更具竞争力.采用托马斯扩展模型结合物质转移阻力对实验结果进行了验证,模拟结果与实验非常符合.

关键词:余氯吸附;颗粒活性炭碳;等温吸附模型;多介质过滤;枣椰仁

中图分类号:X703.5